Compact Wideband High-Selectivity Filtering Power Divider Using Four-Coupled-Lines

Yan ZHANG, Hongmei LIU, Shuo LI, Zhongbao WANG, Shaojun FANG

School of Information Science and Technology, Dalian Maritime University, Dalian, Liaoning 116026, China

zhangyan50050@dlmu.edu.cn, lhm323@dlmu.edu.cn

Submitted November 4, 2024 / Accepted January 8, 2025 / Online first March 4, 2025

Abstract. *In the paper, a compact wideband filtering power divider (FPD) with high frequency selectivity is presented, which is merely based on the four-coupled-lines (FCLs) and isolated resistors. Since the FCL with diagonal short-circuited of input port has filtering response, an FPD without adding extra resonators can be easily realized. Further, two types of FCLs are cascaded as multi-mode resonators for bandwidth enhancement, and two resistors are added for isolation improvement. For validation, a 3-dB prototype with a size of $0.4\lambda_g \times 0.07\lambda_g$ is implemented. Measurements show that the proposed FPD has a fractional bandwidth of more than 80%. Besides, the stopband rejection is over 35 dB with a rectangle coefficient ($|BW_{20dB}/BW_{3dB}|$) of 1.28, which indicates high frequency selectivity.*

Keywords

Filtering power divider (FPD), high selectivity, four-coupled-line (FCL), wideband, miniaturization

1. Introduction

Filtering power divider (FPD) is a fusion component that integrates filter and power divider. Due to the advantages of low IL (IL) and compact size, it is a great candidate in high-integrated systems. Till now, main researches on FPDs include size reduction [1], [2], unequal power division [3], [4], input absorptive [4−6], and wideband [7], [8].

The common method for wideband FPDs is to adopt multi-mode resonators. For example, multi-mode resonators by combining Wilkinson power dividers with coupled-lines (CLs) [9], [10] can achieve the fractional bandwidth (FBW) of nearly 70%, but the circuit sizes are significantly increased. Later, three-coupled-lines are employed for wideband operation [11−13], where size reduction is obtained with maintained wide bandwidth of more than 60%. However, a common issue exists in these FPDs [9−13] that stepped impedance resonators with electrical length of $\lambda_g/2$ are adopted for generating extra transmission zeros (TZs) to realize the high frequency selectivity, which enlarge the overall dimensions significantly.

For high-integrated wireless system applications, a wideband FPD without adding extra resonators is reported [14]. The size reduction of more than 40% is achieved when compared with the FPDs in [11−13]. The only drawback is that the in-band impedance matching is unsatisfactory even with the help of impedance transformer. Thus, the design of wideband high-selectivity FPD with good impedance matching when no extra resonators are inserted is still a challenge.

In the paper, four-coupled-lines (FCLs) are adopted to design the wideband FPD, where high-selectivity can be realized without loading extra resonators and good impedance matching can be maintained. The merits of the proposed FPD include: (1) all-port wideband impedance matching, (2) wide 3-dB bandpass bandwidth (BPBW), (3) wide isolation (IO) bandwidth, (4) high frequency selectivity and large stopband rejection, (5) small size.

2. Theoretical Analysis

2.1 Analysis of the Unequal-width FCL

Figure 1 exhibits the schematic of eight-port unequal-width FCL, which is composed of two outer lines with width of w_1 (called A lines) and two inner lines with width of w_2 (called B lines). The FCL is symmetric about the horizontal centerline MM′. The gaps between adjacent A-B lines are denoted as s_1, and the gap between B-B lines is defined as s_2. The electrical lengths of all CLs in FCL are θ at the center frequency f_0.

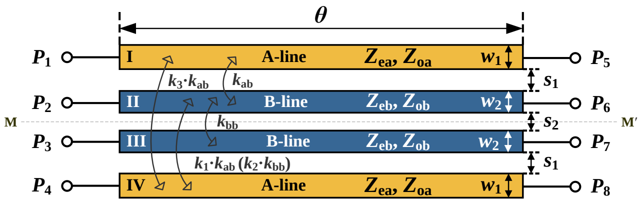

Fig. 1. Schematic of the unequal-width FCL.

DOI: 10.13164/re.2025.0001

$$\mathbf{Z}=\begin{bmatrix} E\alpha & G\alpha & k_1G\alpha & k_3G\alpha & E\beta & G\beta & k_1G\beta & k_3G\beta \\ H\alpha & F\alpha & H\alpha & k_2H\alpha & H\beta & F\beta & H\beta & k_2H\beta \\ k_2H\alpha & H\alpha & F\alpha & H\alpha & k_2H\beta & H\beta & F\beta & H\beta \\ k_3G\alpha & k_1G\alpha & G\alpha & E\alpha & k_3G\beta & k_1G\beta & G\beta & E\beta \\ E\beta & G\beta & k_1G\beta & k_3G\beta & E\alpha & G\alpha & k_1G\alpha & k_3G\alpha \\ H\beta & F\beta & H\beta & k_2H\beta & H\alpha & F\alpha & H\alpha & k_2H\alpha \\ k_2H\beta & H\beta & F\beta & H\beta & k_2H\alpha & H\alpha & F\alpha & H\alpha \\ k_3G\beta & k_1G\beta & G\beta & E\beta & k_3G\alpha & k_1G\alpha & G\alpha & E\alpha \end{bmatrix} \tag{1}$$

where

$$E=\frac{Z_{\mathrm{ea}}+Z_{\mathrm{oa}}}{2},\quad F=\frac{Z_{\mathrm{eb}}+Z_{\mathrm{ob}}}{2},\quad G=\frac{Z_{\mathrm{ea}}-Z_{\mathrm{oa}}}{2}, \tag{2a}$$

$$H=\frac{Z_{\mathrm{eb}}-Z_{\mathrm{ob}}}{2},\quad \alpha=-\mathrm{j}\cot\theta,\quad \beta=-\mathrm{j}\csc\theta. \tag{2b}$$

According to voltage-current method [15], the **Z** matrix of FCL can be derived in (1). In which, the even- and odd-mode characteristic impedances of A-line are Z_{ea} and Z_{oa}, separately. While the corresponding parameters of B-line are Z_{eb} and Z_{ob}, respectively. k_1 is the coupling coefficient ratio between non-adjacent A-B lines (I-III or II-IV lines in Fig. 1) and adjacent A-B lines (I-II or III-IV lines), k_2 is the coupling coefficient ratio between non-adjacent A-B lines and B-B lines (II-III lines), k_3 is the coupling coefficient ratio between A-A lines (I-IV lines) and adjacent A-B lines. Apparently, k_3 is less than k_1 and k_2. What's more, the relationship of $Z_{ij}=Z_{ji}$ $(i\neq j)$ holds due to the reciprocity of FCL, thus the equations of $Z_{\mathrm{ea}}-Z_{\mathrm{oa}}=Z_{\mathrm{eb}}-Z_{\mathrm{ob}}$ and $k_1=k_2$ can be obtained according to (1).

2.2 Analysis of the FCL-based FPD

The schematic of the proposed FPD is exhibited in Fig. 2. It is composed of two types of FCLs (the FCL-I in red dashed box and the FCL-II in blue dashed box, respectively) and two isolated resistors. The parameters with subscript 1 (Z_{ea1}, Z_{oa1}, Z_{eb1}, and Z_{ob1}) denote even-odd mode characteristic impedances of FCL-I. While the corresponding parameters for FCL-II are Z_{ea2}, Z_{oa2}, Z_{eb2}, and Z_{ob2}. The electrical lengths of these two types of FCLs are all equal to θ ($\theta=90°$) at the center frequency f_0. Besides, the resistor R_1 is connected between two FCL-Is for IO enhancement, and the resistor R_2 is introduced to FCL-II for avoiding signal crosstalk between the two output ports.

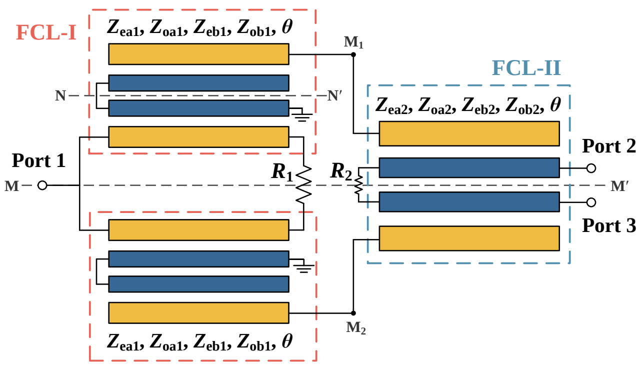

Fig. 2. Schematic of the proposed FCL-based FPD.

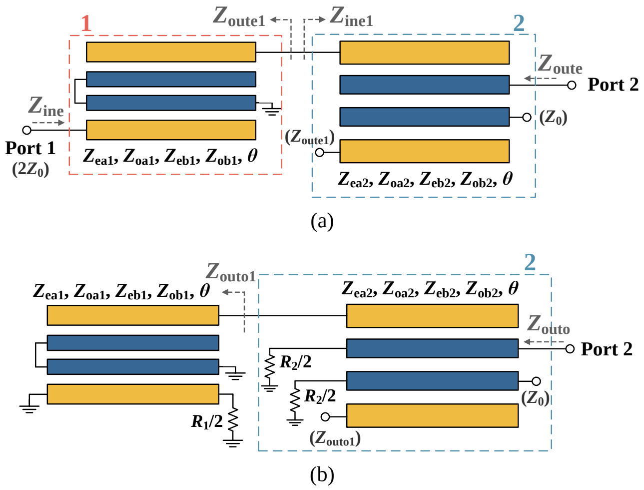

Fig. 3. Sub-circuits of the proposed FPD: (a) even-mode; (b) odd-mode.

Using even-odd mode decomposition method, the proposed FPD can be decomposed of two sub-circuits, as shown in Fig. 3. It is noted that the III- and IV-lines of FCL-II are retained after even-odd mode decomposition to reduce errors [15−17]. Then, the port impedances (Z_{ine}, Z_{oute}, and Z_{outo}) for even-odd mode sub-circuits can be expressed in (3). Here, $Z_{ij}^{1\mathrm{e}}$ $(i, j=1, 2)$ are Z-parameters for the two-port network with red dashed box in Fig. 3(a), $Z_{ij}^{2\mathrm{e}}$ and $Z_{ij}^{2\mathrm{o}}$ are Z-parameters of the two-port network with blue dashed box in Figs. 3(a) and 3(b), separately. In addition, the detailed expressions of $\mathbf{Z}^{1\mathrm{e}}$, $\mathbf{Z}^{2\mathrm{e}}$, $\mathbf{Z}^{2\mathrm{o}}$, Z_{ine1}, Z_{oute1}, and Z_{outo1} are provided in (4) bellow Fig. 6.

$$Z_{\mathrm{ine}}=Z_{11}^{1\mathrm{e}}-\frac{Z_{12}^{1\mathrm{e}}Z_{21}^{1\mathrm{e}}}{Z_{22}^{1\mathrm{e}}+Z_{\mathrm{ine1}}}, \tag{3a}$$

$$Z_{\mathrm{oute}}=Z_{22}^{2\mathrm{e}}-\frac{Z_{12}^{2\mathrm{e}}Z_{21}^{2\mathrm{e}}}{Z_{11}^{2\mathrm{e}}+Z_{\mathrm{oute1}}}, \tag{3b}$$

$$Z_{\mathrm{outo}}=Z_{22}^{2\mathrm{o}}-\frac{Z_{12}^{2\mathrm{o}}Z_{21}^{2\mathrm{o}}}{Z_{11}^{2\mathrm{o}}+Z_{\mathrm{outo1}}}. \tag{3c}$$

According to the input impedances listed in (3), the S-parameters of the proposed FPD can be expressed in (5).

$$S_{11}=\frac{Z_{\mathrm{ine}}-Z_0}{Z_{\mathrm{ine}}+Z_0},\quad S_{23}=\frac{Z_0\left(Z_{\mathrm{oute}}-Z_{\mathrm{outo}}\right)}{\left(Z_{\mathrm{oute}}+Z_0\right)\left(Z_{\mathrm{outo}}+Z_0\right)}, \tag{5a}$$

$$S_{22}=S_{33}=\frac{Z_{\mathrm{oute}}Z_{\mathrm{outo}}-Z_0^2}{\left(Z_{\mathrm{oute}}+Z_0\right)\left(Z_{\mathrm{outo}}+Z_0\right)}, \tag{5b}$$

$$S_{21}=S_{31}=\frac{\sqrt{2}Z_{21}^{1\mathrm{e}}Z_{21}^{2\mathrm{e}}}{\left[\begin{array}{l}\left(Z_{11}^{1\mathrm{e}}+Z_{22}^{2\mathrm{e}}+Z_0+\dfrac{Z_{11}^{1\mathrm{e}}Z_{22}^{2\mathrm{e}}}{Z_0}\right)\left(Z_{11}^{2\mathrm{e}}+Z_{22}^{1\mathrm{e}}\right)\\ -\left(\dfrac{Z_{11}^{1\mathrm{e}}}{Z_0}+1\right)Z_{12}^{2\mathrm{e}}Z_{21}^{2\mathrm{e}}-\left(\dfrac{Z_{22}^{2\mathrm{e}}}{Z_0}+1\right)Z_{12}^{1\mathrm{e}}Z_{21}^{1\mathrm{e}}\end{array}\right]}. \tag{5c}$$

Since the numbers of variables exceed the equations, the optimization method (particle swarm optimization) is adopted as an aid for calculation. Equation (6) gives the optimization objective function O_b. Here, k denotes transmission coefficient of the FPD, N is the sampling number, and f_i is the i-th sampling frequency. During optimization, design goals are assigned for achieving wideband operation, where the FBWs of input and output return loss (RL), IO, and passband are both more than 70%.

$$O_{\mathrm{b}} = \frac{1}{N}\left\{ \begin{array}{l} \sum_{i=1}^{N} \left| S_{11}(f_i)_{\mathrm{dB}} \right|^2 + \sum_{i=1}^{N} \left| S_{22}(f_i)_{\mathrm{dB}} \right|^2 \\ + \sum_{i=1}^{N} \left| S_{23}(f_i)_{\mathrm{dB}} \right|^2 + \sum_{i=1}^{N} \left| S_{21}(f_i)_{\mathrm{dB}} + k \right|^2 \end{array} \right\} \tag{6}$$

As an example, a prototype with equal power distribution ($k = 3$ dB) is designed. Following lists one group of parameters after optimization: $Z_{ea1} = 140\ \Omega$, $Z_{oa1} = 35\ \Omega$, $Z_{eb1} = 135\ \Omega$, $Z_{ob1} = 30\ \Omega$, $Z_{ea2} = 130\ \Omega$, $Z_{oa2} = 25\ \Omega$, $Z_{eb2} = 135\ \Omega$, $Z_{ob2} = 30\ \Omega$, $R_1 = 150\ \Omega$, and $R_2 = 200\ \Omega$. Figure 4 gives normalized theory results of the designed prototype based on the optimized parameters. It can be observed that the input/output RLs are both over 10 dB in the range of $0.4f_0$ to $1.37f_0$ (73%), and the FBW for IO between output ports reaches 78% ($0.61f_0$–$1.39f_0$). Moreover, the 3-dB passband FBW is 87% ($0.57f_0$–$1.44f_0$), and the rectangle coefficient (RC) is 1.24 with the stopband rejection of over 35 dB.

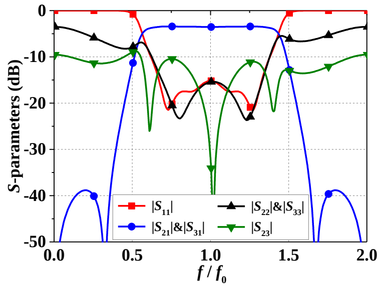

Fig. 4. Theoretical S-parameters of the proposed FPD.

3. Parametric Investigation

In this section, the parameters that have major influences on the FPD are analyzed for better illustration.

3.1 Effects of the FCL-I

Firstly, the main parameters in FCL-I are investigated, including ΔZ_1 ($\Delta Z_1 = Z_{ea1} - Z_{oa1} = Z_{eb1} - Z_{ob1}$), Z_{oa1}, and Z_{ob1}. Figure 5 shows their effects on port impedance matchings. It is noted that the changing trends of impedance matching curves are similar for varying ΔZ_1 and Z_{ob1}. As shown in Figs. 5(a)–5(d), when ΔZ_1 or Z_{ob1} increases, the port RLs are firstly improved and then deteriorated. However, the $|S_{11}|$ at the center frequency f_0 remains constant as Z_{oa1} increases, but the bandwidth ($|S_{11}| < -10$ dB) is varied. At the output port, the $|S_{22}|$ at f_0 is increased with Z_{oa1}, thus affecting the bandwidth.

Since the FCL with diagonal short-circuited of input port can generate four TZs [18], [19], the positions of TZs are mainly influenced by the parameters in FCL-I. Figures 6(a) and 6(b) exhibit the effects of Z_{oa1} and Z_{ob1} on output performance. In which, Z_{oa1} has almost no influence on the positions of TZs, but the stopband rejection is improved as Z_{oa1} increases. The positions of TZs can be slightly varied by Z_{ob1}, and the stopband rejection is first improved and then deteriorated when Z_{ob1} increases.

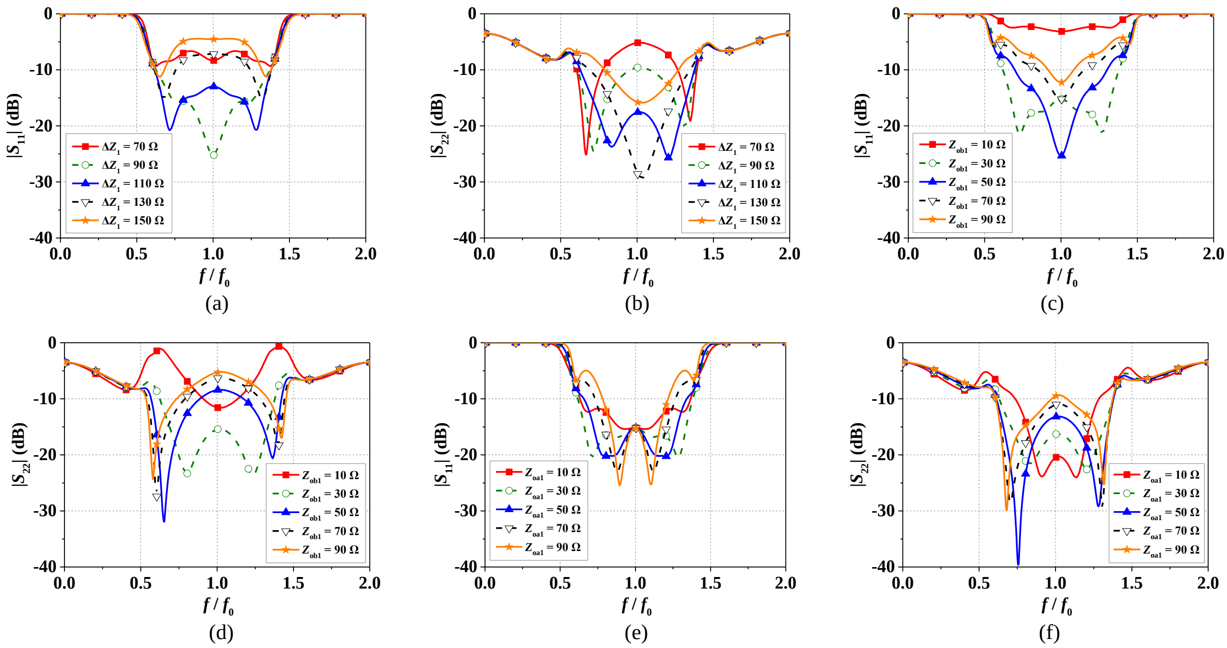

Fig. 5. (a) Effects of ΔZ_1 on $|S_{11}|$. (b) Effects of ΔZ_1 on $|S_{22}|$. (c) Effects of Z_{ob1} on $|S_{11}|$. (d) Effects of Z_{ob1} on $|S_{22}|$. (e) Effects of Z_{oa1} on $|S_{11}|$. (f) Effects of Z_{oa1} on $|S_{22}|$.

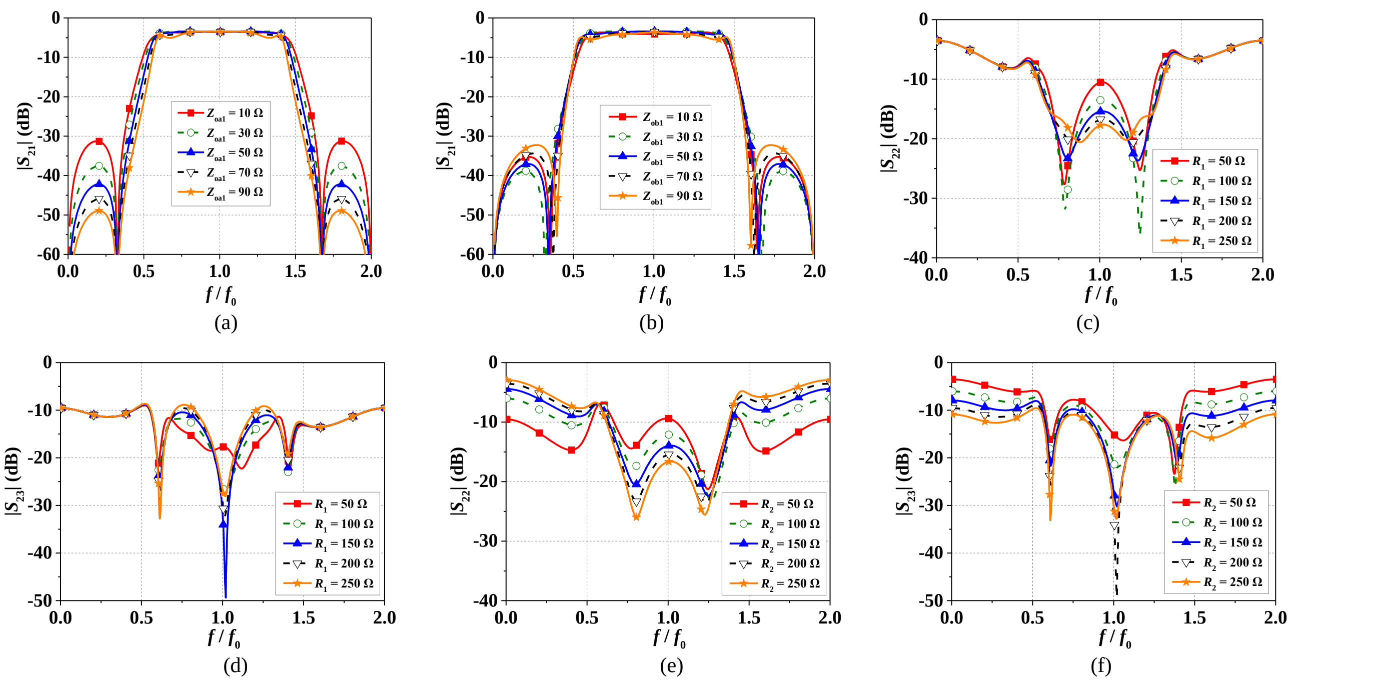

Fig. 6. (a) Effects of Z_{oa1} on $|S_{21}|$. (b) Effects of Z_{ob1} on $|S_{21}|$. (c) Effects of R_1 on $|S_{22}|$. (d) Effects of R_1 on $|S_{23}|$. (e) Effects of R_2 on $|S_{22}|$. (f) Effects of R_2 on $|S_{23}|$.

$$Z_{\text{ine1}} = Z_{11}^{2\text{e}} - \frac{Z_{12}^{2\text{e}} Z_{21}^{2\text{e}}}{Z_{22}^{2\text{e}} + Z_0}, \quad Z_{\text{oute1}} = Z_{22}^{1\text{e}} - \frac{Z_{12}^{1\text{e}} Z_{21}^{1\text{e}}}{Z_{11}^{1\text{e}} + 2Z_0}, \tag{4a}$$

$$Z_{\text{outo1}} = \frac{Y_{55}Y_{87} - Y_{57}Y_{85} - \left\{\left[Y_{85}\left(Y_{27} - Y_{37}\right) + Y_{87}\left(Y_{25} - Y_{35}\right)\right] \cdot \left[Y_{58}Y_{87} - Y_{57}\left(Y_{88} + R_1/2\right)\right]\right\}}{Y_{87}\left[Y_{87}\left(Y_{28} - Y_{38}\right) - \left(Y_{27} - Y_{37}\right)\left(Y_{88} + R_1/2\right)\right]}, \tag{4b}$$

$$Y_{mn} = \frac{\left[\begin{array}{c} Z_{44}\left[Z_{mn}\left(Z_{72} - Z_{73}\right) - Z_{7n}\left(Z_{m2} - Z_{m3}\right)\right] + \left(Z_{42} - Z_{43}\right)\left(Z_{m4}Z_{7n} - Z_{74}Z_{mn}\right) \\ + Z_{4n}\left[Z_{74}\left(Z_{m2} - Z_{m3}\right) - Z_{m4}\left(Z_{72} - Z_{73}\right)\right] \end{array}\right]}{Z_{44}\left(Z_{72} - Z_{73}\right) - Z_{74}\left(Z_{42} - Z_{43}\right)}, \tag{4c}$$

$$\begin{bmatrix} Z_{11}^{1\text{e}} & Z_{12}^{1\text{e}} \\ Z_{21}^{1\text{e}} & Z_{22}^{1\text{e}} \end{bmatrix} = \begin{bmatrix} X_{44} - \dfrac{\left(X_{42} - X_{43}\right)\left(X_{24} - X_{34}\right)}{X_{22} - X_{23} - X_{32} + X_{33}} & X_{45} - \dfrac{\left(X_{42} - X_{43}\right)\left(X_{25} - X_{35}\right)}{X_{22} - X_{23} - X_{32} + X_{33}} \\ X_{54} - \dfrac{\left(X_{52} - X_{53}\right)\left(X_{24} - X_{34}\right)}{X_{22} - X_{23} - X_{32} + X_{33}} & X_{55} - \dfrac{\left(X_{52} - X_{53}\right)\left(X_{25} - X_{35}\right)}{X_{22} - X_{23} - X_{32} + X_{33}} \end{bmatrix}, \quad X_{mn} = Z_{mn} - \frac{Z_{m7}Z_{7n}}{Z_{77}}, \tag{4d}$$

$$\begin{bmatrix} Z_{11}^{2\text{e}} & Z_{12}^{2\text{e}} \\ Z_{21}^{2\text{e}} & Z_{22}^{2\text{e}} \end{bmatrix} = \begin{bmatrix} X_{11} - \dfrac{X_{14}X_{41}}{X_{44} + Z_{\text{oute1}}} & X_{16} - \dfrac{X_{14}X_{46}}{X_{44} + Z_{\text{oute1}}} \\ X_{61} - \dfrac{X_{64}X_{41}}{X_{44} + Z_{\text{oute1}}} & X_{66} - \dfrac{X_{64}X_{46}}{X_{44} + Z_{\text{oute1}}} \end{bmatrix}, \quad U_{mn} = W_{mn} - \frac{W_{3n}W_{m3}}{W_{33} + \dfrac{R_2}{2}}, \tag{4e}$$

$$\begin{bmatrix} Z_{11}^{2\text{o}} & Z_{12}^{2\text{o}} \\ Z_{21}^{2\text{o}} & Z_{22}^{2\text{o}} \end{bmatrix} = \begin{bmatrix} U_{11} - \dfrac{U_{14}U_{41}}{U_{44} + Z_{\text{outo1}}} & U_{16} - \dfrac{U_{14}U_{46}}{U_{44} + Z_{\text{outo1}}} \\ U_{61} - \dfrac{U_{64}U_{41}}{U_{44} + Z_{\text{outo1}}} & U_{66} - \dfrac{U_{64}U_{46}}{U_{44} + Z_{\text{outo1}}} \end{bmatrix}, \quad W_{mn} = X_{mn} - \frac{X_{2n}X_{m2}}{X_{22} + \dfrac{R_2}{2}} \tag{4f}$$

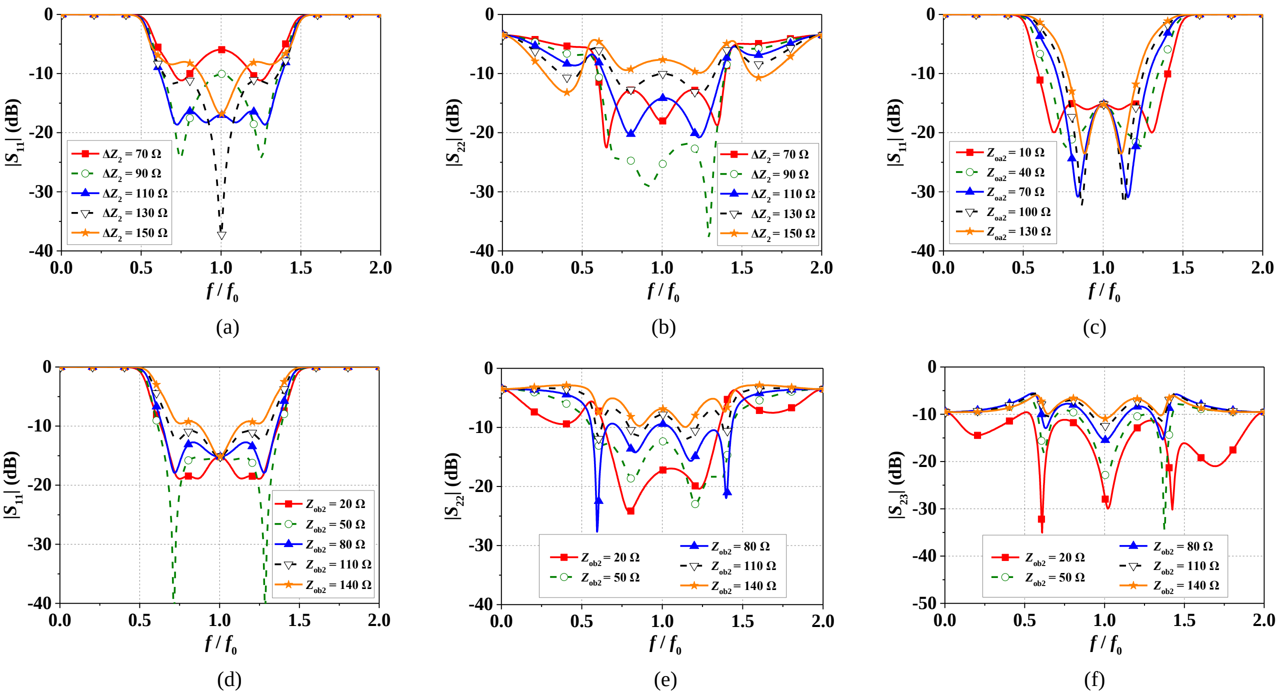

Fig. 7. (a) Effects of ΔZ_2 on $|S_{11}|$. (b) Effects of ΔZ_2 on $|S_{22}|$. (c) Effects of Z_{oa2} on $|S_{11}|$. (d) Effects of Z_{ob1} on $|S_{11}|$. (e) Effects of Z_{ob2} on $|S_{22}|$. (f) Effects of Z_{ob2} on $|S_{23}|$.

3.2 Effects of the Resistors

The effects of isolated resistors (R_1 and R_2) on output port impedance matching ($|S_{22}|$) and isolation ($|S_{23}|$) are discussed, as shown in Figs. 6(c)–6(f). It is seen that the $|S_{22}|$ at f_0 gets better as R_1 or R_2 increases. While the effects of R_1 or R_2 on $|S_{23}|$ are contrary. Thus, a trade-off should be done on R_1 and R_2 in consideration of both impedance matching and isolation.

3.3 Effects of the FCL-II

Similarly, the parameters ΔZ_2, Z_{oa2}, and Z_{ob2} in FCL-II are studied. Figure 7 gives their effects on impedance matchings and isolations. Here, the trends of $|S_{11}|$ and $|S_{22}|$ are similar as ΔZ_2 increases, which are both first improved and then deteriorated. Moreover, Z_{oa2} and Z_{ob2} have the same effects on the input impedance matching, where the bandwidth is narrowed as Z_{oa2} or Z_{ob2} increases. Z_{ob2} also has significant influences on $|S_{22}|$ and $|S_{23}|$. It can be observed from Figs. 7(f) and 7(f) that smaller Z_{ob2} is preferred.

4. Implementation and Measurements

For validation, a prototype operating at 2 GHz is designed and fabricated. Firstly, the relations between theory parameters and physical dimensions are introduced. According to Z_{ea} and Z_{oa}, the width w_a and gap s_a of A-line-based CLs can be calculated. Similarly, the width w_b and gap s_b of B-line-based CLs can be obtained based on Z_{eb} and Z_{ob}. Then, the widths of A-line (w_1) and B-line (w_2) in FCL are approximately equal to w_a and w_b, separately. The gap s_1 in FCL is approximately equal to s_a, and the gap s_2 is approximately the average of s_a and s_b [17]. By using Rogers 4350b substrate ($\varepsilon_r = 3.48$, $\tan\delta = 0.0037$, $h = 1.524$ mm), a model is optimized in Ansoft HFSS. Figure 8 presents the layout and photograph of the fabricated prototype, where the overall size is 60 mm × 11 mm ($0.4\lambda_g \times 0.07\lambda_g$).

The prototype is measured on Agilent N5230A network analyzer. It can be observed from Fig. 9(a) that the measured FBW of input impedance bandwidth is 80% (1.25–2.85 GHz), exhibiting good impedance matching. The measured output power distribution is 3.54 dB at f_0, and the 3-dB passband ranges from 1.25 GHz to 2.85 GHz (88%). Besides, the fabricated prototype achieves a RC of 1.28 with stopband rejection of over 35 dB. It can be observed from Fig. 9(b) that within the range from 1.04 GHz to 2.76 GHz (86%), the measured output RL and IO are both more than 10 dB. Moreover, the designed FPD also has

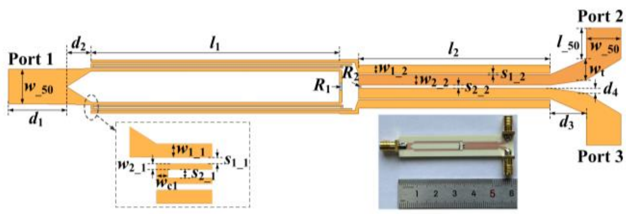

Fig. 8. Layout and photograph of the fabricated FPD. ($w_{1\_1} = 0.24$ mm, $w_{2\_1} = 0.1$ mm, $w_{1\_2} = 0.8$ mm, $w_{2\_2} = 1$ mm, $w_t = 2$ mm, $s_{1\_1} = 0.11$ mm, $s_{2\_1} = 0.15$ mm, $s_{1\_2} = 0.12$ mm, $s_{2\_2} = 0.3$ mm, $l_1 = 24$ mm, $l_2 = 18.5$ mm, $d_1 = 5.6$ mm, $d_2 = 1.5$ mm, $d_3 = 3.5$ mm, $d_4 = 0.5$ mm, $R_1 = 150\ \Omega$, $R_2 = 200\ \Omega$).

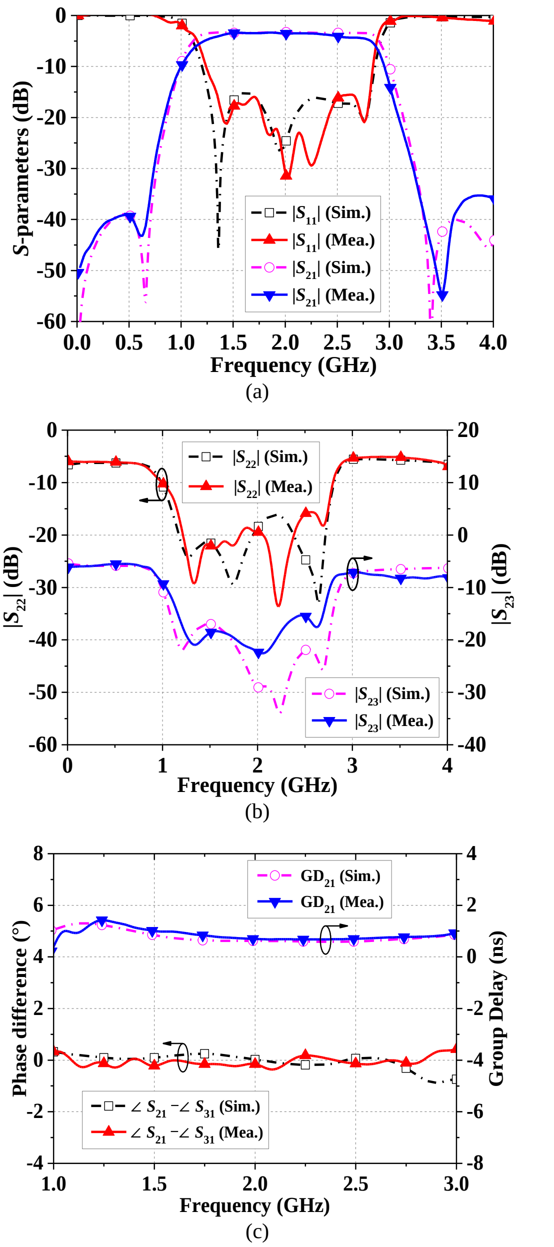

Fig. 9. Simulated and measured results of the fabricated prototype. (a) $|S_{11}|$ and $|S_{21}|$. (b) $|S_{22}|$ and $|S_{23}|$. (c) Phase difference between output ports and group delay.

a flat output phase difference (< ±1°) between the two output ports, as shown in Fig. 9(c). The simulated and measured group delay (GD) are also plotted in Fig. 9(c), where the measured GD is less than 1 ns within the operated bandwidth.

The comparisons between the proposed and reported wideband FPDs are summarized in Tab. 1. Compared with the representative FPDs, the proposed FPD has the widest overlapped bandwidth, lowest IL, and highest frequency selectivity. Besides, it also owns advantages of good in-band impedance matching, large stopband rejection, and compact size.

Ref.	[9]	[12]	[13]	[14]	**This work**
f_0 (GHz)	3.9	2.08	3	2.42	**2**
Overlapped FBW[a] (%)	63.6	65.4	62	62	**80**
In-band $\|S_{11}\|$ (dB)	≤ −14.6	≤ −20	≤ −16	≤ −12	**≤ −16**
IL (dB)	0.74	0.71	0.6	0.8	**0.54**
RC	1.35	1.38	1.43	1.45	**1.28**
Stopband rejection (dB)	> 40	> 28	> 29	> 35	**> 35**
Add extra resonators	Y	Y	Y	N	**N**
Technique	MMR	MMR	MMR	SMR	**MMR**
Size ($\lambda_g \times \lambda_g$)	0.47×0.29	0.43×0.21	0.5×0.25	0.32×0.05	**0.4×0.07**

[a]: 10-dB input/output RL & 10-dB IO & 3-dB BPBW; IL: insertion loss; RC: rectangle coefficient=$|BW_{20dB}/BW_{3dB}|$; MMR: Multi-mode resonator; SMR: Single-mode resonator.

Tab. 1. Comparisons between the proposed and reported wideband FPDs.

5. Conclusions

In the paper, a compact wideband FPD with high frequency selectivity is presented by utilizing the inherent feature of FCL. Measured results demonstrate that the proposed FPD exhibits an overlapped FBW of 80%, a RC of 1.28, and a stopband rejection of more than 35 dB. Since wideband filtering with high frequency selectivity can be achieved without extra resonators, size reduction can be realized simultaneously, which indicates its potential applications in highly integrated wireless communication systems.

Acknowledgments

This work was supported in part by the National Natural Science Foundation of China under Grant 52471371, in part by the Liaoning Revitalization Talents Program under Grant XLYC2007067, in part by the Young Elite Scientists Sponsorship Program by China Association for Science and Technology under Grant 2022QNRC001, and in part by the China Scholarship Council under Grant 202406570025.

References

[1] SHEN, G. X., CHE, W. Q., XUE, Q., et al. Novel design of miniaturized filtering power dividers Using Dual-Composite Right-/Left-Handed Resonators. *IEEE Transactions on Microwave Theory and Techniques*, 2018, vol. 66, no. 12, p. 5260–5271. DOI: 10.1109/TMTT.2018.2873313

[2] FENG, T., MA, K. X., WANG, Y. Q. A miniaturized bandpass filtering power divider using quasi-lumped elements. *IEEE Transactions on Circuits and Systems II: Express Briefs*, 2022, vol. 69, no. 1, p. 70−74. DOI: 10.1109/TCSII.2021.3087699

[3] GUO, X., LIU, Y. H., WU, W. Wideband unequal filtering power divider with arbitrary constant power ratio and phase difference. *IEEE Transactions on Circuits and Systems II: Express Briefs*, 2023, vol. 70, no. 2, p. 421−425. DOI: 10.1109/TCSII.2022.3212675

[4] ZHANG, S. R., LIU, H. M., CHEN, S. Y., et al. Wideband filtering power divider with unequal power division ratio and all-Frequency input absorptive feature. *IEEE Transactions on Circuits and Systems II: Express Briefs*, 2024, vol. 71, no. 3, p. 1136−1140. DOI: 10.1109/TCSII.2023.3324915

[5] ZHU, Y. H., CAI, J., CAO, Y., et al. Compact wideband absorptive filtering power divider with a reused composite T-shape network. *IEEE Transactions on Circuits and Systems II: Express Briefs*, 2023, vol. 70, no. 3, p. 899−903. DOI: 10.1109/TCSII.2022.3217462

[6] ZHANG, Y. F., WU, Y. L., YAN, J., et al. Wideband high-selectivity filtering all-frequency absorptive power divider with deep out-of-band suppression. *IEEE Transactions on Plasma Science*, 2021, vol. 49, no. 7, p. 2099−2106. DOI: 10.1109/TPS.2021.3083780

[7] ZHAO, W., WU, Y. L., YANG, Y. H., et al. Novel on-chip wideband filtering power dividers with high selectivity and ultra-wide out-of-band suppression in LTCC technology. *IEEE Transactions on Circuits and Systems II: Express Briefs*, 2022, vol. 69, no. 11, p. 4288−4292. DOI: 10.1109/TCSII.2022.3179308

[8] WANG, X. D., GUO, Z. C., WANG, J. P., et al. Synthesis design of a self-packaged wideband out-of-phase filtering power divider implemented by PCB lamination process. *IEEE Transactions on Components, Packaging and Manufacturing Technology*, 2023, vol. 13, no. 11, p. 1833−1839. DOI: 10.1109/TCPMT.2023.3327686

[9] XIAO, J. K., YANG, X. Y., LI, X. F. A 3.9GHz/63.6% FBW multi-mode filtering power divider using self-packaged SISL. *IEEE Transactions on Circuits and Systems II: Express Briefs*, 2021, vol. 68, no. 6, p. 1842−1846. DOI: 10.1109/TCSII.2020.3048108

[10] WANG, Y. C., XIAO, F., CAO, Y., et al. Novel wideband microstrip filtering power divider using multiple resistors for port isolation. *IEEE Access*, 2019, vol. 7, p. 61868−61873. DOI: 10.1109/ACCESS.2019.2913093

[11] XIA, Z. P., WANG, J. P., LU, Q. Y., et al. A wideband 90° phase shifting element applied in quadrature phase filtering power divider. *IEEE Microwave and Wireless Technology Letters*, 2024, vol. 34, no. 2, p. 167−170. DOI: 10.1109/LMWT.2023.3340720

[12] TIAN, H. Y., XIAO, L. K., YU, H., et al. Wideband microstrip filtering power divider designed by direct synthesis technique (DST). *IEEE Microwave and Wireless Components Letters*, 2022, vol. 32, no. 6, p. 507−510. DOI: 10.1109/LMWC.2022.3143546

[13] YU, X., SUN, S. A novel wideband filtering power divider with embedding three-line coupled structures. *IEEE Access*, 2018, vol. 6, p. 41280−41290. DOI: 10.1109/ACCESS.2018.2858275

[14] XU, K. D., BAI, Y. C., REN, X., et al. Broadband filtering power dividers using simple three-line coupled structures. *IEEE Transactions on Components, Packaging and Manufacturing Technology*, 2019, vol. 9, no. 6, p. 1103−1110. DOI: 10.1109/TCPMT.2018.2869077

[15] LIU, H. M., MA, Y. H., GUAN, M. Y., et al. Synthesis of miniaturized wideband four-way filtering power divider consisting of unequal-width three-coupled-lines. *International Journal of RF and Microwave Computer-Aided Engineering*, 2021, vol. 31, no. 10. DOI: 10.1002/mmce.22805

[16] ZHANG, S. R., LIU, H. M., CHEN, S. Y., et al. Synthesis of wideband all-frequency absorptive filtering power divider with high selectivity and flat output port distributions. *Electronics*, 2023, vol. 12, no. 17, p. 1–16. DOI: 10.1002/electronics.12173704

[17] CHEN, C. P., KATO, N., ANADA, T. Synthesis scheme for wideband filters consisting of three-coupled-lines including the cross-coupling between non-adjacent lines. *IET Microwave Antennas Propagation*, 2015, vol. 9, no. 14, p. 1558−1566. DOI: 10.1049/IET-MAP.2014.0467

[18] LI, L., LI, Z. F. Side-coupled shorted microstrip line for compact quasi-elliptic wideband bandpass filter design. *IEEE Microwave and Wireless Components Letters*, 2010, vol. 20, no. 6, p. 322−324. DOI: 10.1109/LMWC.2010.2047516

[19] ZHU, H., ABBOSH, A., GUO, L. Ultra-wideband unequal in-phase power divider using three-line coupled structure. *Electronic Letters*, 2014, vol. 50, no. 15, p. 1081–1082. DOI: 10.1049/el.2014.1214

About the Authors ...

Yan ZHANG was born in Shanxi, China. She received the B.S. degree in Communication Engineering from Dalian Jiaotong University (DJTU), China, in 2018, and the Master degree in Electronic and Communication Engineering from Dalian Maritime University (DMU), China, in 2021. She is currently pursuing the Ph.D. degree at DMU. Her research interests include function fusion microwave circuits and beamforming networks.

Hongmei LIU (corresponding author) received the Ph.D. degree in Information and Communication Engineering from Dalian Maritime University (DMU), China, in 2016. She is currently a Full Professor with the School of Information Science and Technology, DMU. Her current research interests include CP antennas, multi-function microwave circuits, reconfigurable RF components, and multi-beam antennas. She has authored or co-authored over 90 papers in journals and conferences. She is currently serving as a Technical Reviewer for the IEEE Transactions on Microwave Theory and Techniques, IEEE Transactions on Circuits and Systems, IEEE Transactions on Industrial Electronics, IEEE Microwave and Wireless Components Letters, IET Microwaves, Antennas & Propagation, International Journal of RF and Microwave Computer-Aided Engineering, and AEU-International Journal of Electronics and Communications. She was a recipient of the Best Doctor's Dissertation Award of Liaoning Province in 2017.

Shuo LI was born in Hebei, China. She received the B.S. degree in Information Engineering from East China Jiaotong University (ECJTU), Jiangxi, China, in 2022. She is currently working toward the Doctor degree at Dalian Maritime University (DMU). Her current research interests include filtering component, reconfigurable circuits and beamforming network.

Zhongbao WANG received the Ph.D. degree in Communication and Information Systems from DMU, China, in 2012. He is currently a Full Professor with the School of Information Science and Technology, DMU. From 2014 to 2018, he was a Postdoctoral Fellow with Beijing Univ. of Posts and Telecommunications, China. From 2019 to 2020, he was a Visiting Scholar with National Univ. of Singapore, Singapore. He has authored more than 90 journal papers. He is currently serving as a Technical Reviewer for the IEEE Transactions on Circuits and Systems, MTT, MWTL, Radioengineering, etc. His current research interests include balanced RF components and CP antennas.

Shaojun FANG received the Ph.D. degree in Communication and Information Systems from Dalian Maritime University (DMU), Liaoning, China, in 2001. Since 1982, he has been at DMU, where he is currently the Head Professor with the School of Information Science and Technology. His recent research interests include passive RF components, patch antennas, and computational electromagnetics. He has authored or co-authored three books and over 100 journal and conference papers. He was a recipient of the Best Doctor's Dissertation Award of Liaoning Province in 2002 and the Outstanding Teacher Award of the Ministry of Transport of China.